



Cite this: *Nanoscale Horiz.*, 2022, 7, 1161

# Inkjet printing of two-dimensional van der Waals materials: a new route towards emerging electronic device applications

Kyungjune Cho,<sup>\*a</sup> Takhee Lee <sup>b</sup> and Seungjun Chung <sup>\*ac</sup>

Two-dimensional (2D) van der Waals (vdW) materials are considered one of the most promising candidates to realize emerging electrical applications. Although until recently, much effort has been dedicated to demonstrating high-performance single 2D vdW devices, associated with rapid progress in 2D vdW materials, demands for their large-scale practical applications have noticeably increased from a manufacturing perspective. Drop-on-demand inkjet printing can be the most feasible solution by exploiting the advantages of layered 2D contacts and advanced 2D vdW ink formulations. This review presents recent achievements in inkjet-printed 2D vdW material-based device applications. A brief introduction to 2D vdW materials and inkjet printing principles, followed by various ink formulation methods, is first presented. Then, the state-of-the-art inkjet-printed 2D vdW device applications and their remaining technical issues are highlighted. Finally, prospects and challenges to be overcome to demonstrate fully inkjet-printed, high-performance 2D vdW devices are also discussed.

Received 30th March 2022,  
Accepted 14th July 2022

DOI: 10.1039/d2nh00162d

rsc.li/nanoscale-horizons

## Introduction

The upcoming “Internet of Everything”, which will enable our surrounding electronics to be closely interconnected, has accelerated the development of next-generation electronics based on emerging materials.<sup>1–5</sup> In recent years, two-dimensional (2D) van der Waals (vdW) materials have been regarded as one of the most promising candidates owing to their superior properties,

<sup>a</sup> Soft Hybrid Materials Research Center, Korea Institute of Science and Technology, Seoul 02792, Korea. E-mail: kcho@kist.re.kr, seungjun@kist.re.kr

<sup>b</sup> Department of Physics and Astronomy, and Institute of Applied Physics, Seoul National University, Seoul 08826, Korea

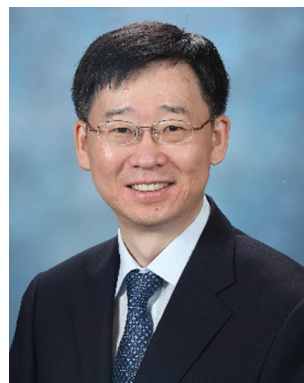
<sup>c</sup> KHU-KIST Department of Converging Science and Technology, Kyung Hee University, Seoul, 02447, Korea



**Kyungjune Cho**

interests include emerging low-dimensional materials and their interfaces. He has been highly productive during his career with over 50 research publications.

*Kyungjune Cho received his PhD degree from the Department of Physics and Astronomy, Seoul National University in 2019, and then he was a postdoctoral researcher at the Department of Nano-systems from Ions, Spins and Electrons, Max Planck Institute of Microstructure Physics, Halle, Germany, until 2021. He is now a postdoctoral researcher at the Korea Institute of Science and Technology (KIST), Seoul, Republic of Korea. His current research*



**Takhee Lee**

*self-assembled monolayers, polymers, semiconductor nano-materials, and their assembly into electronic devices. He edited 2 books and wrote 11 book chapters, 18 review articles, and more than 300 journal articles.*

*Takhee Lee is a Professor in the Department of Physics and Astronomy, Seoul National University, Korea. He received his BS and MS degree in physics at Seoul National University in 1992 and 1994, respectively, and he received his PhD degree in physics at Purdue University, USA, in 2000. He was a postdoctor at Yale University, USA until 2004. His current research interests are characterization of the electrical properties of structures involving molecular*

including electrical, optical, and even mechanical characteristics. Specifically, their inherently different electrical and optoelectronic behaviours when thinned down to the atomic limit by exploiting either physical or chemical exfoliation methods have attracted significant attention from both research and industrial societies. In addition to well-known pioneering materials in the field of 2D vdW materials, *e.g.*, graphene (Gr) and semiconducting transition metal dichalcogenides (TMDs), various novel vdW materials have been discovered, which can be used as superconductors, ferro- and antiferromagnets, topological insulators, and Weyl semimetals.<sup>6–17</sup>

Notably, their recent advances to realize practical applications have been encouraged beyond single device demonstration, initiating vibrant research for cost-effective, large-area, and high-yield mass production. In this sense, omnipresent inkjet printing has been employed as a feasible solution to meet the aforementioned demands of large area, low cost, easy processability, and high compatibility. In addition, inkjet printing can offer a high degree of design freedom for 2D nanoelectronics while maintaining their high electrical performance.<sup>18–26</sup> 2D vdW material-based inks are also suitable for use in inkjet printing as active pigments due to the rapid progress in the ink formulation methodology from synthesis of 2D vdW materials to novel electrochemical exfoliation methods. Moreover, inkjet printing of 2D vdW layered nanosheet pigments has attractive advantages in layer-by-layer stacking from the device performance perspective over other materials such as zero-dimensional (0D) quantum dots and one-dimensional (1D) nanowires.<sup>27–29</sup> To create transport channels for active layers, for instance, electrodes and semiconducting channels, the printed low-dimensional nanocomposites must be interconnected with neighbouring dots/wires/sheets to transport charge carriers. When nanocomposites are interconnected, energy barriers are inevitably formed at the contact regions; therefore, tackling such inherent contacts is significantly important to improve the charge

transport properties. As depicted in Fig. 1a, 0D quantum dot-based nanocomposites form point contacts, resulting in high energy barriers. From a mesoscopic perspective, the size of the 0D system also gives rise to a large number of point contacts, resulting in high channel resistance. For 1D nanocomposite channels, although there would also be high energy barriers from point contacts among wires, higher conductivity compared to 0D systems can be delivered, which would be coupled with a lower number of point contacts (Fig. 1b). Interestingly, 2D nanocomposites have shown the possibility of achieving much higher conductivity, creating 2D contacts connected layer-by-layer due to the capillary force between neighbouring sheets corresponding to much lower energy barriers, as shown in Fig. 1c. Although matured inkjet-printed 1D nanowire (NW)-based devices have shown better overall electronic performances as of now,<sup>30</sup> it has been believed that inkjet-printed 2D electronics have a huge potential owing to their intrinsic advantages over 1D and 0D films, such as higher surface coverage, lower barrier density, and lower barrier height from their structural nature. Moreover, manufacturing heterostructures of 2D materials with varying material combinations, thicknesses, and structures are also feasible.<sup>27</sup> Therefore, for emerging inkjet-printed devices with low-dimensional materials, 2D layered nanosheets are the most favourable for demonstrating a well-stacked channel *via* drop-on-demand deposition without complicated alignment processing (Fig. 1d). Note that alignment techniques, *e.g.*, shear rolling, have been widely employed in 1D nanowire systems for better electrical performance. Utilizing these advantages, various inkjet-printed 2D vdW material-based emerging devices, such as sensors, photodetectors, thermoelectrics, wearable electronics, and even superconducting devices, have been vigorously investigated.<sup>5,18,21,22,31–44</sup> In this regard, many researchers have reported noteworthy results in novel ink formulation methods and inkjet-printed emerging device applications over the last decade. Representatively, Kelly *et al.* reported all-inkjet-printed thin-film transistors (TFTs) with layered 2D Gr, WSe<sub>2</sub>, and boron nitride (BN) as an electrode, a semiconductor, and insulating layers, respectively (Fig. 1e).<sup>45</sup>

This minireview highlights recent achievements in inkjet-printed 2D vdW material-based devices from conventional TFTs to the most recently reported Josephson junction device. The overarching aim is to show the feasibility of realizing emerging 2D layered devices associated with inkjet printing and provide an overview of recent efforts to improve their electrical performance. We hereby assume that the time is right to summarize the progress in inkjet printing of 2D vdW materials, especially from the perspective of 2D ink preparation with a suitable inkjet printing strategy, and the state-of-the-art device applications in line with the latest trends in 2D electronics.

## 2D vdW ink formulation methods

### Pigments: representative 2D vdW materials

To establish an inkjet printing strategy, the formulation of a rheologically well-designed ink is the starting point. Before discussing the rheological principles and methodology for ink



**Seungjun Chung**

*Seungjun Chung received his PhD degree from the Department of Electrical Engineering and Computer Science, Seoul National University in 2012, and then he was a postdoctoral researcher at the Department of Electrical Engineering and Computer Sciences, University of California, Berkeley until 2016. He is now a principal research scientist at the Korea Institute of Science and Technology (KIST), Seoul, Republic of Korea. His current research interests include additive manufacturing for advanced stretchable electronics and emerging low-dimensional semiconductor devices. He has been highly productive during his career with over 80 research publications, and 40 domestic and foreign Patents.*

*Seungjun Chung received his PhD degree from the Department of Electrical Engineering and Computer Science, Seoul National University in 2012, and then he was a postdoctoral researcher at the Department of Electrical Engineering and Computer Sciences, University of California, Berkeley until 2016. He is now a principal research scientist at the Korea Institute of Science and Technology (KIST), Seoul, Republic of Korea. His current research interests include additive manufacturing for advanced stretchable electronics and emerging low-dimensional semiconductor devices. He has been highly productive during his career with over 80 research publications, and 40 domestic and foreign Patents.*

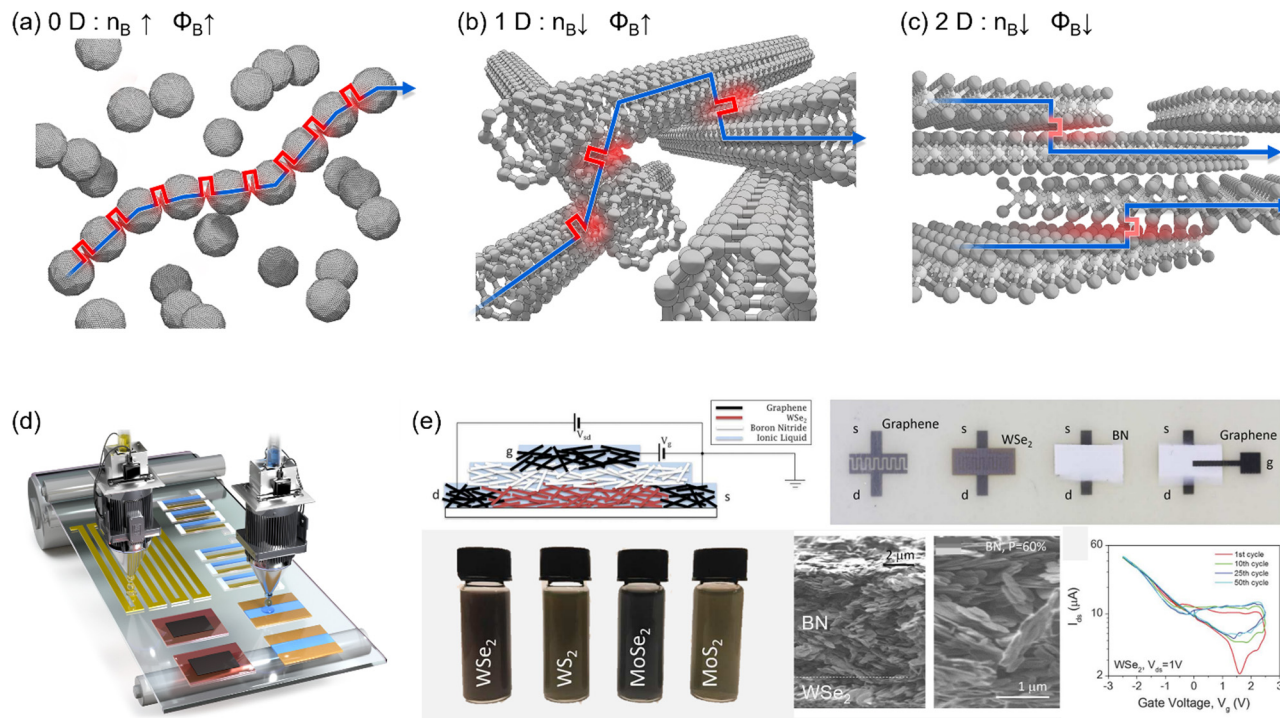


**Fig. 1** (a) The conducting path through connected 0D nanoparticles includes a large number of point contacts with neighbouring nanoparticles, with high energy barriers. (b) The conducting path through 1D nanowires includes a dramatically reduced number of point contacts with high energy barriers. (c) The conducting path through 2D nanosheets includes a greatly reduced number of sheet contacts with also greatly reduced the energy barrier due to the large contact area. (d) Schematic image of the fabrication of various electronic devices by using inkjet printing. (e) 2D vdW-based field-effect transistor and its transfer curves. Reproduced with permission.<sup>45</sup> Copyright 2017, Publisher AAAS.

formulation, we first focus on the 2D vdW material pigments. As the 2D vdW family has been intensively investigated due to its attractive properties, remarkable developments in the field of vdW material synthesis from bulk crystals to large-area monolayers have also been achieved. In particular, conventional synthesis methods, *e.g.*, molecular beam epitaxy (MBE), and chemical vapour deposition (CVD), have enabled the synthesis of large-area monolayers comparable to high-quality bulk crystals synthesized by chemical vapour transport (CVT).<sup>6,7,31,46–51</sup> Owing to these continued efforts and progress, a variety of large-area synthesized 2D vdW materials now exhibit attractive physical properties. In addition to representative semimetallic Gr, insulating hexagonal BN (h-BN), semiconducting TMDs (*e.g.*, MoS<sub>2</sub> and WSe<sub>2</sub>), and metallic TiS<sub>2</sub>, we now have magnetic (CrI<sub>3</sub>, CrCl<sub>3</sub>, CrBr<sub>3</sub>, Fe<sub>3</sub>GeTe<sub>2</sub>, *etc.*) and even superconducting (NbSe<sub>2</sub> and Bi<sub>2</sub>Te<sub>3</sub>) vdW materials.<sup>52–62</sup> In particular, their layer-dependent energy band structures and the feasibility of fabricating clean heterostructures without lattice mismatch concerns accelerate the progress in exploring both in-depth material characteristics and optimized device fabrication.<sup>11,52,53,63,64</sup>

The energy band structure of a 2D vdW material is tuneable by adjusting prominent parameters, such as the number of layers.<sup>65</sup> Additionally, even the stacking angles of a heterostructure were found to possibly act as a key factor in modulating the band structure since they can introduce an additional periodic potential to the system by forming a moiré lattice.<sup>66–68</sup>

Additional functionalities, *e.g.*, superconductivity of Gr<sup>68</sup> or ferroelectricity of twisted h-BN,<sup>66</sup> can also be delivered by introducing the vdW transfer technique. The absence of dangling bonds on the surface of 2D vdW materials and their weak vdW interactions between layers provide promising opportunities to fabricate heterostructures with atomically clean interfaces with different neighbouring 2D layers. With these advantages, atomically clean heterostructures with a variety of vdW material combinations can be realized by employing advanced fabrication methodologies, such as the polydimethylsiloxane (PDMS)-based vdW dry transfer method.<sup>69</sup> For example, insulating h-BN can be used to encapsulate underlying air-sensitive 2D materials, and Gr can be used as a contact to enhance the charge injection due to its high conductivity and low density of states near the Fermi level.<sup>52,53</sup> In particular, owing to the rapid progress in the vdW transfer technique, the field of twistronics has been opened. As a result, superconducting 1.1° twisted bilayer Gr has become the most well-known twisted homobilayer system, also called “magic-angle” Gr.<sup>67</sup> These 2D vdW heterostructures have been widely studied in a variety of research fields, not only limited to electronics but also including thermoelectrics, magnetism, spintronics, and topology.<sup>9,12,50,70–77</sup>

From the 2D vdW material perspective, much effort has been dedicated to synthesizing and discovering new vdW materials exhibiting various electrical properties, as shown in Fig. 2. For example, although magnetism is one of the most important natures, in-depth research begun relatively recently due to the

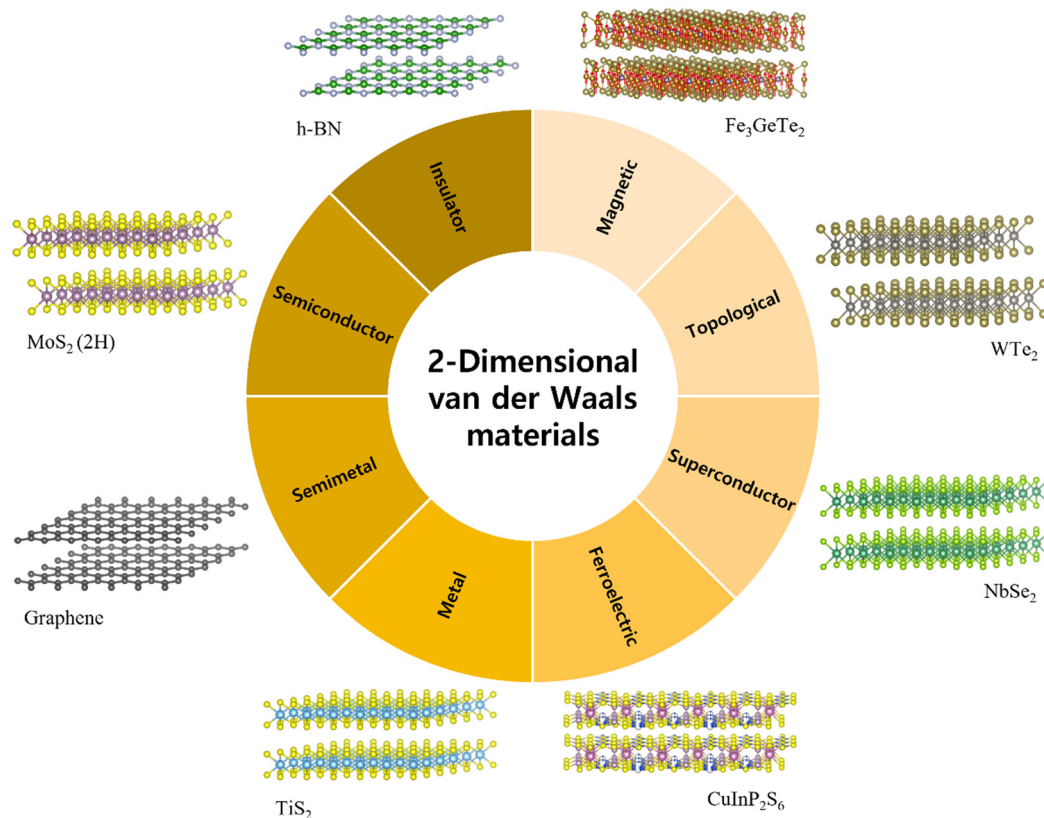


Fig. 2 Schematic illustration of functional 2D vdW materials.

limited intrinsically magnetic vdW materials. As a result of continued efforts to find and synthesize magnetic vdW materials, studies on magnetism-related research including spintronics of 2D magnetic vdW materials have been initiated.<sup>9,49,56,58,76,78,79</sup>

In addition, the 2D heterostructure platform has a strong advantage without the lattice mismatch concern, while fabricating magnetic heterostructures by using conventional magnetic materials and device fabrication is difficult due to lattice distortion, which can also distort the magnetic dipole alignment. Similarly, research on 2D topological insulators and Weyl semimetals has begun, as they have recently discovered.<sup>62,75–77</sup>

However, the results of these emerging materials are still limited to a single device fabricated by using mechanical exfoliation methods, which are not suitable for practical applications. Due to the strong motivation for transitioning from proof-of-concept to large-scale application, drop-on-demand inkjet printing has become a strong candidate from a manufacturing perspective because it offers high resolution, less material waste, and a wide range of substrate compatibility as well as noncontact and maskless processability. Specifically, layer-by-layer contacts of 2D vdW materials can be readily demonstrated by using inkjet printing, which can presumably create a significant synergistic effect with the advantages of 2D vdW materials.<sup>21,24,26</sup> In this frame, significant efforts have been devoted to adapting 2D vdW materials to inkjet printing to meet these demands and extend the boundaries of technologies.

### Principles of 2D vdW ink formulation and inkjet printing

**Liquid phase exfoliation (LPE) methods.** For 2D vdW ink formulation, liquid exfoliation from bulk crystals, usually assisted by electrochemical and ultrasonic processes, is the most well-known approach to preparing pigments for inkjet printing. In addition, it enables the extraction of a sufficient amount of 2D vdW flakes on demand. In contrast to bulk crystals, uniformly grown monolayers synthesized *via* MBE or CVD cannot typically be sufficient material sources for ink formulation due to the relatively low density of 2D flakes. Generally, it has been known that the undesirable strain can be induced due to the lattice mismatch during the bottom-up synthesis process resulting in undesirable defects and non-uniform crystal orientations with a lot of grain boundaries. However, although this substrate effect may also affect the CVT-grown bulk crystals, it has been known that the CVT-grown bulk crystals usually exhibit better quality since the CVT method requires high reaction time and temperature which can offer sufficient energy and time for crystallization and homogeneous element distribution.<sup>80</sup>

Therefore, high-quality bulk crystals of 2D materials have been widely grown *via* CVT prior to exfoliation.<sup>6,7,49,51</sup> As illustrated in Fig. 3a, CVT generally uses two temperature zones in a vacuum-sealed ampul: (1) a hot zone where the source materials are placed and (2) a cool zone where the synthesized bulk crystals are deposited after the chemical reaction (note that they can be reversed if the chemical reaction

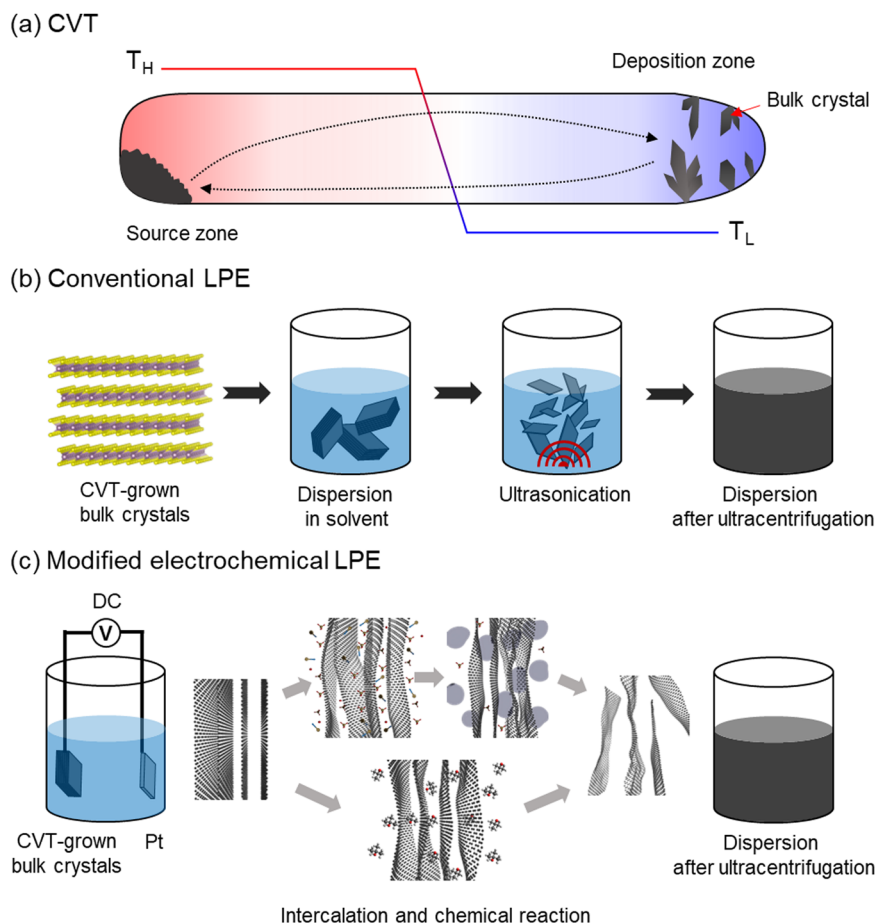


**Fig. 3** (a) Schematic illustration of the CVT synthesis method with two different temperature zones. The source materials heated in the hot zone are transported as a gas phase, depositing in the cool zone as a crystal phase. (b) Schematic illustration of the LPE method. (c) Schematic illustration of the electrochemically assisted LPE method. The electrochemical exfoliation generally involves ion intercalation inducing delamination.

for synthesis is endothermic). After the synthesis process, the deposited bulk crystals are removed from the ampul and placed on an electrode (anode or cathode) in an ionic liquid solvent for the next step, electrochemical exfoliation. This involves exfoliation from a wide range of 2D vdW bulk crystals induced by the external energy, such as mechanical energy from ultrasonication, or driven by an electrochemical reaction in a target solvent. LPE can be utilized to produce a wide range of 2D vdW material-based inks.<sup>81,82</sup> In detail, the weak layer-by-layer interaction can be easily broken by the introduction of external stress, intercalation of ions between layers, or creation of bubbles through chemical reactions of intercalated ions, resulting in isolated free-standing mono- or few layers in the target solvents.

At the early stage of the LPE method, as illustrated in Fig. 3b, the bulk crystal pieces are just placed in the solvent, followed by ultrasonication to promote exfoliation in the liquid. Then, the 2D vdW material dispersed in the solvent is generally subjected to multiple centrifugations to selectively collect free-standing layers with a target thickness or size. Importantly, because the condition of the applied external force, *e.g.*, the strength of the ultrasonication wave or the exposure time, can determine

the average size of free-standing flakes, corresponding to the quality of 2D flakes, it should be carefully optimized to prevent their severe destruction. In addition, after the exfoliation process, the delaminated 2D flakes can aggregate.

To overcome these hurdles, additional processes have been proposed, for example, the aforementioned electrochemical reactions or ion intercalations. The electrochemical exfoliation strategy entails an external voltage bias along with ionic solvents that have ion intercalants in them so that ions can migrate from the solvent to the electrode where the bulk crystal is located.<sup>83–88</sup> Consequently, the ions intercalate into the gaps between the layers of the bulk crystal, as shown in Fig. 3c. In summary, the intercalated ions located between the layers broaden the interlayer distance, weakening the weak vdW interaction and thus promoting delamination. Sometimes, air bubbles are intentionally produced between the layers as byproducts of induced electrochemical reactions during the chemical reactions. Such chemically created air bubbles grow larger as the chemical reaction continuously progresses. Eventually, they physically push away neighbouring layers, stimulating delamination of bulk crystals. Note that the bulk crystal can be placed on either the anode side or cathode side

depending on the intercalants (*i.e.*, positive ions or negative ions) used for exfoliation. These should be carefully determined depending on the purposes because ionic intercalants often introduce additional defects to the 2D vdW crystals or promote unwanted oxidation and lattice distortions.<sup>89</sup> In addition, intercalated ions can prevent potential aggregation without additives. These methods generally require milder ultrasonication than in conventional LPE because the vdW interactions between the layers are already weakened by ions and bubbles or often do not require ultrasonication at all. Then, centrifugation can be performed for dispersion purposes. Therefore, these approaches promise a higher chance of producing large-area, less-defective high-quality flakes in 2D vdW inks, which can lead to a higher electronic performance of printed devices.

### Inkjet printing of 2D vdW inks

Drop-on-demand (DOD) inkjet printing can eject out 2D vdW inks from nozzles to underlying layers, so it is one of the most promising candidates for direct film deposition without a complicated etching process. There are two representative types of printing systems, which have a nozzle based on (a) a piezoelectric actuator or (b) a thermal heater to form ink droplets and drive the jetting force, as illustrated in Fig. 4a.<sup>90–92</sup> In the case of inkjetting by a piezoelectric actuator, extrinsic voltage pulses are applied to the piezoelectric transducer located in the nozzle, and in turn, the moving membrane of the transducer creates pressure pulses that are applied to the ink inside the nozzle. Likewise, air bubbles can be created by Joule heating from thermal nozzles, and the evaporated gas also forms ink droplets and creates pressure for jetting. However, in the latter case, the range of the solvent is limited because the ink solution should be volatile to reliably create the desired size

of bubbles. Therefore, water or short-chain alcohols are typically considered ink solvents for thermal actuator systems, while a wide range of solvents can be employed in piezoelectric actuator systems. In addition, the ink ejection in response to the pressure generated by the piezoelectric element can allow relatively good resolution, requiring lower temperature compared to the thermal counterpart, which suffers from ink degradation concerns and temperature-sensitive solvent choice. For these reasons, piezoelectric nozzles are more frequently adopted for state-of-the-art emerging applications using DOD inkjet printing.

To pursue the best printing quality, the rheology of the ink must also be delicately controlled since the rheological properties of inks play a central role in DOD inkjet printing. In other words, the interfacial properties and rheological parameters of 2D vdW inks, such as density, surface tension, and viscosity, should be carefully considered to promote high-quality printed layers. According to previous studies, the following conditions are empirically required for a well-formulated ink that is good in terms of stability and printability. First, to avoid nozzle clogging, the average size of dispersed pigments, the vdW nanoflakes, should be less than 1/50 of the nozzle diameter.<sup>33,93</sup> Additionally, the viscosity dominantly influences the microfluidic dynamics of the ink droplets. For example, if the viscosity is too high, then the ink droplets will not be easily ejected from the nozzle. In contrast, if the viscosity is too low, then the droplet will not be stabilized and consequentially form satellite drops. For these reasons, the suitable viscosity range is known to be 1–25 mPa s<sup>-1</sup>. Similarly, 20–50 mN m<sup>-1</sup> surface tension has been suggested to avoid difficulties in inkjetting from nozzles. Owing to prolonged efforts, these rheological parameters have been merged into two dimensionless numbers, the Reynolds number (Re), which is known to predict flow patterns, and the Weber number (We), which is used to analyse

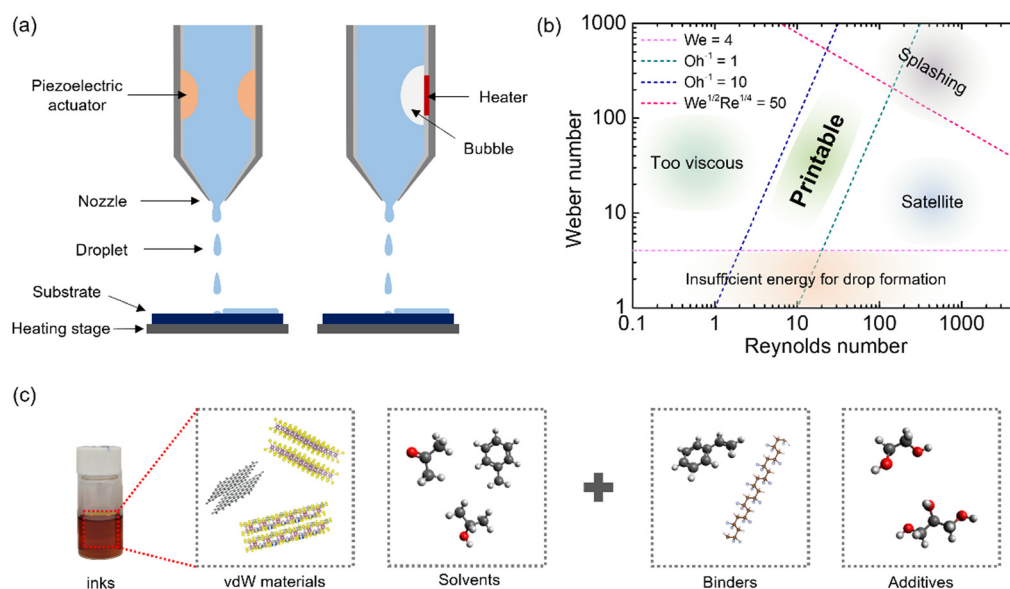


Fig. 4 (a) Two representative types of nozzles for inkjet printing with different actuators: a piezoelectric transducer and a heater. (b) Rheological parameters and expected printability. (c) General compositions of 2D vdW inks.

fluid flows, written as follows:

$$\text{Re} = \frac{\rho v d}{\eta}$$

$$\text{We} = \frac{\rho v^2 d}{\gamma}$$

where  $\rho$  is the density and  $v$  is the velocity of the jetted ink,  $d$  is the diameter of the nozzle,  $\eta$  is the viscosity of the ink, and  $\gamma$  is the ink surface tension.<sup>94,95</sup> These two numbers have been known to account for the formation of droplets. Note that such conditions and numbers have been found empirically and cannot be an absolute criterion. Likewise, when the velocity is too low and the surface tension is too high such that the droplet cannot overcome the surface tension barrier ( $\text{We} < 4$ ), droplets would not be formed in flight. In addition, to precisely predict the quality of inkjetting, another dimensionless number  $Z$ , the inverse of the Ohnesorge number ( $\text{Oh} = \text{We}^{1/2}/\text{Re}$ ),

$$Z = \text{Oh}^{-1} = \frac{\text{Re}}{\sqrt{\text{We}}} = \frac{\sqrt{\rho v d}}{\eta}$$

has been generally employed. Note that  $Z$  does not require the fluid velocity; thus, it can only explain the physical properties of the fluid and the characteristic length.<sup>94</sup> According to previous studies, the suitable range of  $Z$  values to avoid poor inkjetability, *e.g.*, not ejecting or forming satellite droplets, is approximately 1 to 10.<sup>97</sup>

As we discussed, since the quality of inkjetting affects the quality of printed features, not only exfoliation approaches for preparing 2D vdW inks from bulk crystals but also suitable solvent systems should be carefully chosen to create well-defined ink droplets. Additionally, binders or additives may be involved in ink solvents to elaborately control their rheological parameters to achieve higher stability and printability of 2D vdW inks without forming particle agglomerates or settled flakes. Binders can assist to improve the adhesion and

mechanical stability of printed inks by binding them together. Additives generally refer to any other additives that can be added to modulate the rheological properties of inks for better printability. Taking into account such important rheological parameters, 2D vdW material-based inks have been successfully formulated in various solvents, as shown in Fig. 5a and b, with novel electrochemical exfoliation techniques.<sup>43,96</sup> Zeng *et al.* also claimed that they could stabilize an aqueous vdW ink by using surface-active Gr quantum dot nanosurfactants (NanoS), as shown in Fig. 5c, while the dispersed flakes tended to reaggregate without NanoS.<sup>99</sup>

Again, 2D vdW materials are naturally favoured for inkjet printing by creating layered 2D contacts. As a host of vdW materials, including ternary and even quaternary families, have been newly discovered and synthesized, many researchers have put in a great deal of effort to fully exploit the aforementioned advantages and produce stable and printable inks for emerging large-area applications. For further developments, continuing efforts in formulating rheologically well-designed air-stable 2D vdW inks are encouraged.

### Emerging inkjet-printed 2D vdW device electronic applications

Beyond the single device perspective, the realization of large-area applications based on 2D vdW materials has attracted much attention. At this point, inkjet printing is believed to be a cornerstone of achieving this goal since the attractive advantages of both 2D vdW materials and inkjet printing can create synergetic effects. Based on these reasons, many researchers have combined inkjet printing methodologies and 2D vdW materials. From various passive components, such as conducting electrodes and even a superconducting channel, to active devices, such as all-printed transistors, sensors, and sophisticated circuits, many emerging applications have been proposed, expanding the boundaries in terms of both materials and inkjet printing techniques. Therefore, in this section, we will summarize and discuss recent progress.

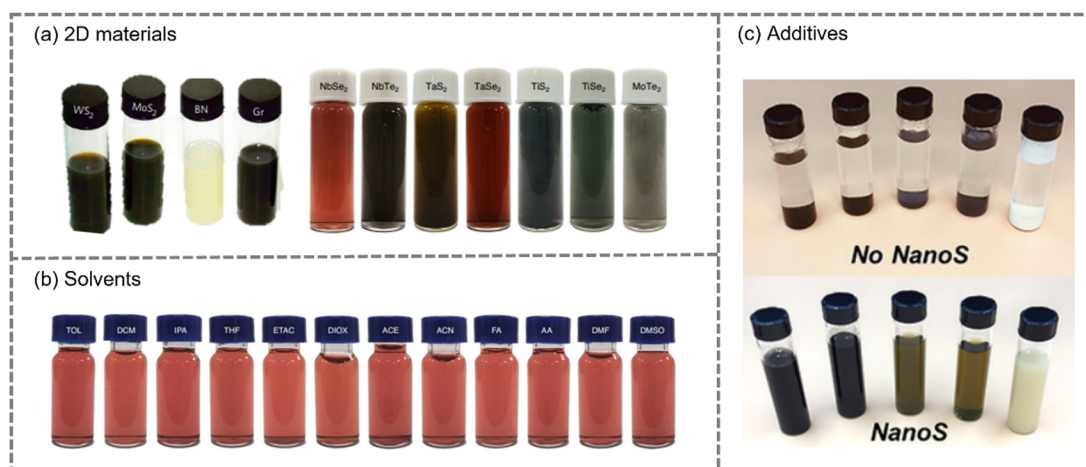


Fig. 5 (a) Formulated inks with various 2D vdW materials. Reproduced with permission. (Left<sup>98</sup> Copyright 2017, Right<sup>44</sup> Copyright 2021, respectively), Publisher Springer Nature. (b) 2D vdW inks with various solvents. Reproduced with permission.<sup>44</sup> Copyright 2021, Publisher Springer Nature. (c) Example of additives that prevent reaggregation. Reproduced with permission.<sup>99</sup> Copyright 2020, Publisher Wiley-VCH.

### Inkjet-printed 2D Gr-based electronic devices

In the early stage of the field of printed devices with 2D vdW materials, the demonstration of a single device component such as an electrode, an active channel, and a dielectric layer was usually attempted. As various 2D vdW inks can be formulated, many researchers have been interested in how to realize fully printed active devices or circuit applications with 2D vdW materials. As a result, all-printed devices have been recently reported to be fabricated with representative 2D vdW materials such as Gr and h-BN. For example, Carey *et al.* successfully fabricated fully printed 2D material-based field-effect transistors (FETs) and circuits on textiles for wearable electronics.<sup>33</sup> They used an ink formulation method based on solvent exchange. Firstly, the bulk 2D crystals were effectively exfoliated in a high-boiling point solvent because these solvents can suspend 2D materials without additional stabilisation agents. Subsequently, the exfoliated 2D materials were transferred to a low boiling-point solvent to utilize their rapid evaporation at room temperature. The fully printed Gr/h-BN heterostructure device, where Gr is the active channel, h-BN is the dielectric layer and poly(3,4-ethylenedioxythiophene) polystyrene sulfonate (PEDOT:PSS) is the electrodes, is shown in Fig. 6a. They achieved average field-effect mobility values of  $150 \pm 15 \text{ cm}^2 \text{ V}^{-1} \text{ s}^{-1}$  on polyethylene terephthalate (PET) and  $91 \pm 29 \text{ cm}^2 \text{ V}^{-1} \text{ s}^{-1}$  on polyester textile. In addition, they could demonstrate fully printed complementary inverter, logic gate, and memory behaviours. However, because the active channel was printed Gr, which is not a semiconducting material, the on/off ratio of printed transistors reached only  $1.23 \pm 0.3$ , and the gain value of the printed inverter was only approximately 0.1. Therefore, even though they demonstrated the possibility of fully printed, flexible, and stretchable devices and logic circuits on textiles, further improvements are needed for utilization in practical applications.

Even if gapless Gr is used as the active layer, combining functional additives can open a new way to demonstrate high-performance devices. Recently, Zeng *et al.* reported that they could formulate stable aqueous inks by adding Gr quantum dot nanosurfactants.<sup>99</sup> The Gr quantum dot (GQD)-added inks could be successfully stabilized in an aqueous system by the reduced surface interfacial tension, showing better printability. Nanoparticle-based surfactants have attracted much attention owing to the synergetic properties of nanoparticles and surfactants. The polyaromatic core structure of the GQD enabled the enhancement of the long-term colloidal stability of graphene ink by introducing the non-covalent  $\pi$ - $\pi$  interactions between Gr and the GQD. Additionally, the GQD was found to be able to effectively reduce the interfacial tension and alleviate the aggregation of nanomaterials in water. With these GQDs, they could formulate stable  $\text{MoS}_2$ ,  $\text{WS}_2$ , Gr, and h-BN inks (Fig. 5c) and fabricate all-printed optoelectronic devices. Not only were post-thermal treatments, which are required when organic surfactants are involved, found to be not required, but also, additional functionality could be introduced due to the bandgap in GQDs attached to the surface of Gr layers. Taking advantage of nanosurfactants, they fabricated

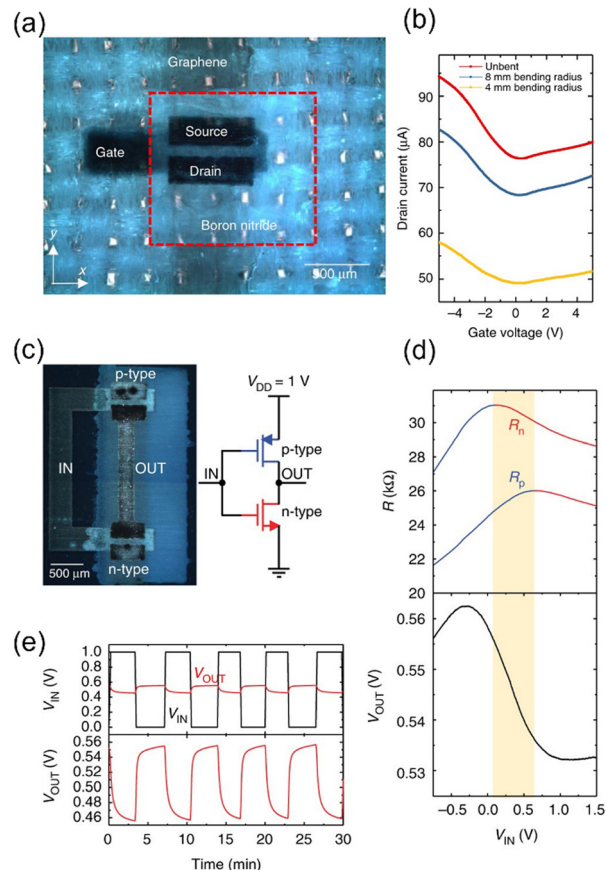


Fig. 6 (a) Optical image of a printed FET. (b) Transfer characteristics of the FET for different bending radii. (c) Optical image of an inkjet-printed integrated circuit. (d) Measured static resistance and measured static voltage transfer characteristics. (e) Digital  $V_{\text{IN}}$  and  $V_{\text{OUT}}$  waveforms measured on an inverter. Reproduced under the terms of the Creative Commons CC BY license.<sup>32</sup>

bandgap-engineered high-performance printed photodetectors with different device structures having the printed GQDs as a different component, *i.e.*, (i) as an active channel in the Ag/GQD-Gr/Ag structure, (ii) as electrodes in the GQD-Gr/GaN/GQD-Gr structure, and (iii) in cross-plane Ag/GQD-Gr/Al (Fig. 7a–c), and all three devices showed a superior photodetection performance compared to previously reported results, as shown in Fig. 7d–f. Furthermore, they demonstrated an array of UV photodetector devices on a hemispherical glass substrate with a radius of 15 mm as a proof-of-concept.

### 2D TMD-based electronic devices with inkjet-printed components

As the development of exfoliation techniques has enabled the preparation of various 2D vdW inks beyond Gr-based inks, inkjet printing of TMDs has begun. Unlike Gr, many members of the TMD family have an intrinsic bandgap energy, providing more options in inkjet-printed semiconducting devices. Among the variety of TMDs, n-type semiconducting  $\text{MoS}_2$  has attracted considerable attention due to its attractive properties, such as tuneable bandgap, superior electronic properties, and strong



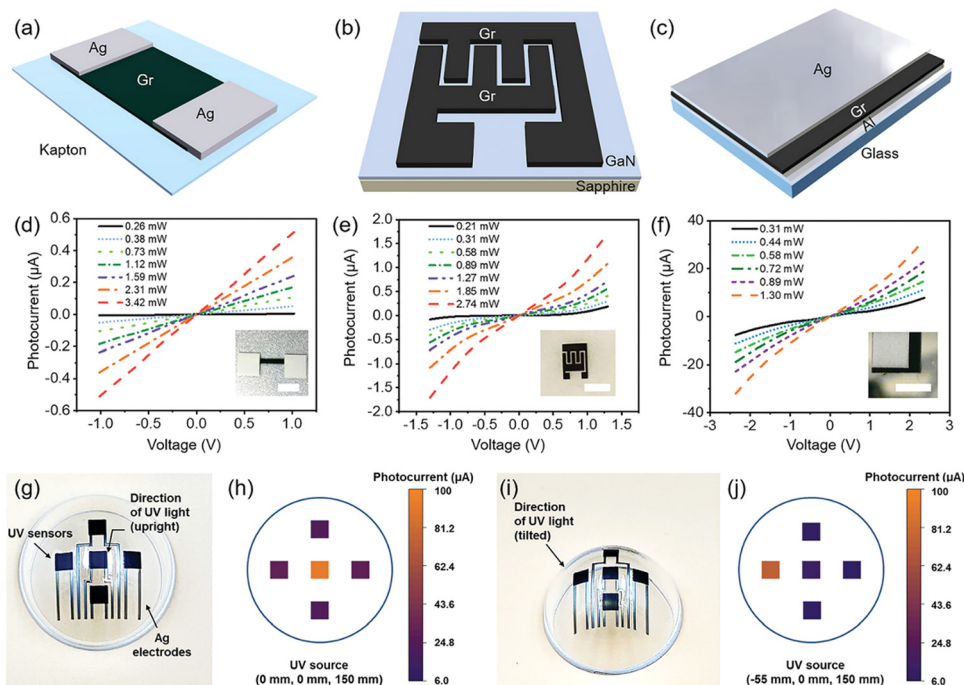
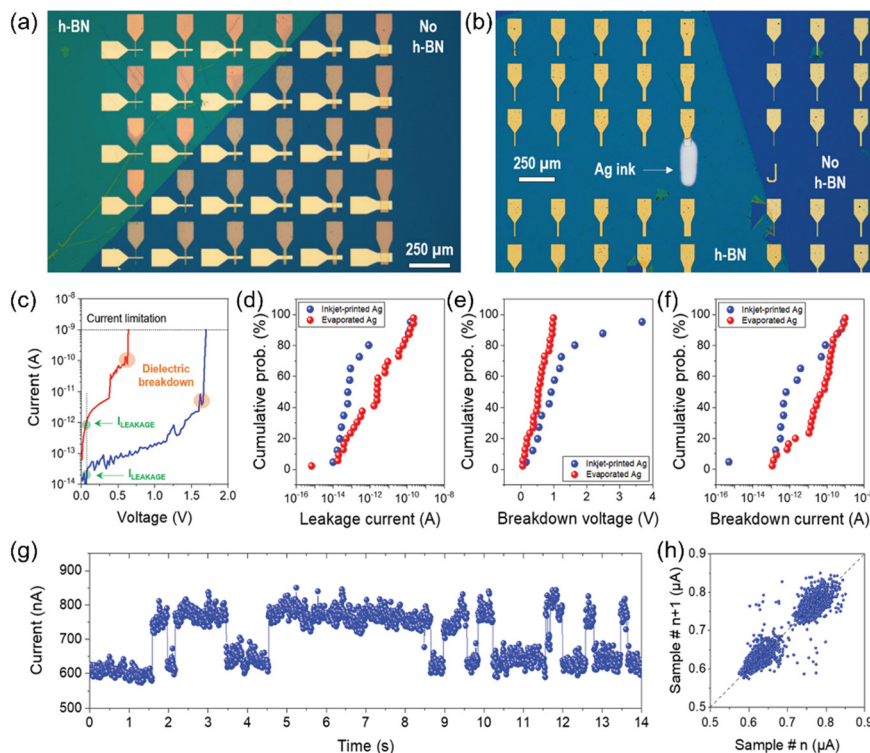


Fig. 7 Printed UV sensors using a nanosurfactant ink. (a) Schematic illustrations of an in-plane device with a Gr active channel and (b) a GaN active channel and of (c) a cross-plane device. (d–f)  $I$ – $V$  curves corresponding to the three UV detectors shown in (a–c), respectively, under UV illumination. (g) and (i) Optical image of an all-printed 3D photodetector array, and photocurrent mapping results under (h) vertical illumination and (j) tilted-angle illumination. Reproduced with permission.<sup>99</sup> Copyright 2020, Publisher Wiley-VCH.

spin-orbit coupling, and has been employed as active channels to overcome the intrinsic limitations of using gapless Gr, as shown in Fig. 1e.<sup>45</sup> Before fully exploiting these TMD inks, an alternative method for realization of large-area applications was proposed: the combination of large-area synthesized TMDs and inkjet printing.<sup>46,100</sup> Inkjet printing-based film deposition can be a strong candidate to form electrical contacts on 2D materials due to the nondestructive nature of inkjet printing. Recently, Zheng *et al.* reported that inkjet printing can be a strategy for defect-free metal deposition on 2D vdW materials.<sup>101</sup> Contact engineering between the metal electrodes and underlying vdW materials has been intensively studied to improve charge injection at the contact to overcome the vdW gap.<sup>52,53,102–105</sup> Additionally, Fermi level pinning effects originating from the interfacial states should be addressed in the field of 2D electronics. According to recent results, high-energy deposition using vacuum evaporation systems may create additional defects at the surface of vdW materials due to high-energy particle collisions that can hinder charge carrier injection and cause the Fermi level pinning effect.<sup>106</sup> However, inkjet printing deposition does not require a high-energy deposition process, resulting in defect-free metal deposition on 2D materials.<sup>101</sup> The authors reported that the metallic contacts deposited using inkjet printing could form a defectless interface with the underlying h-BN layer. Additionally, as shown in Fig. 8a and b, they fabricated metal-insulator-metal (MIM) capacitors with metal organic CVD (MOCVD)-grown h-BN *via* metal deposition by both inkjet printing and evaporation and then compared the electrical breakdown voltages.

Fig. 8c shows the  $I$ – $V$  curves for the MIM structures with inkjet-printed and evaporated electrodes, where green dots indicate the leakage current at 0.1 V and orange dots show the dielectric breakdown voltages. Owing to the less defective interfaces between inkjet-printed metal electrodes and h-BN layers, the leakage current of the MIM structures with evaporated metal electrodes was on average 100 times higher than that of the counterparts with inkjet-printed electrodes, indicating that the average power consumption would also be approximately 100 times higher. Furthermore, the nondestructive nature of inkjet printing metal deposition would be beneficial to improving the charge injection properties of semiconducting 2D vdW materials, which can be a pathway to realizing high-performance 2D vdW material-based electrical applications.

As it has been reported that the inkjet printing approach is highly compatible with large-area grown 2D vdW materials, much effort has been dedicated to employing both large-area synthesized 2D vdW films and inkjet printing for emerging applications. This approach would have several advantages over all-2D vdW inkjet printing in terms of electrical performance and the feasibility of fabrication of 2D monolayer devices. Recently, Conti *et al.* demonstrated high-performance FETs and logic circuits with a CVD-grown MoS<sub>2</sub> active channel and inkjet-printed electrodes.<sup>107</sup> First, they transferred a CVD-grown MoS<sub>2</sub> film onto a paper substrate, which was followed by metal electrode printing. However, for the top gate FETs, another 2D vdW material layer, an h-BN layer, was printed on top of the transferred CVD-grown MoS<sub>2</sub>. Because the n-type semiconducting monolayer MoS<sub>2</sub> intrinsically has a direct



**Fig. 8** Optical image of an array of Ag/MOCVD h-BN/Ag cross-bar devices with top electrodes deposited with (a) electron beam evaporation and (b) inkjet printing. (c) Representative  $I$ - $V$  curves of the devices with top electrodes deposited by electron beam evaporation (red) and inkjet printing (blue). (d-f) Statistical analysis of the leakage current, breakdown voltage, and breakdown current. (g) Stable random telegraph noise (RTN) signal measured in a device with top electrodes deposited by inkjet printing. (h) Weighted scatter plot of the current data evaluated at discrete-time  $i + 1$  vs.  $i$ . Reproduced with permission.<sup>101</sup> Copyright 2021, Publisher Wiley-VCH.

bandgap of 1.9 eV, they could obtain highly enhanced logic gating compared to the all-printed Gr FETs and all-printed MoS<sub>2</sub> FETs shown in Fig. 1e and 6, respectively. The achieved mobility value was  $\sim 0.8 \text{ cm}^2 \text{ V}^{-1} \text{ s}^{-1}$ , and the on/off ratio was found to be  $\sim 3 \times 10^3$ , which is also much higher than the value of  $\sim 25$  for the all-printed MoS<sub>2</sub> FET. Furthermore, they also demonstrated logic gates and current mirrors based on inkjet-printed MoS<sub>2</sub> FETs on paper substrates. As shown in Fig. 9a and b, they fabricated a resistor-transistor logic inverter with a Gr resistor and Ag electrodes, and its gain value was found to be greater than 25. Considering that the gain of the printed Gr inverter was approximately 0.1, as shown in Fig. 6d, the gain was significantly improved by more than 200 times, even though the printed MoS<sub>2</sub> was fabricated on environmentally sustainable and mechanically flexible paper substrates. With the high gain value of the MoS<sub>2</sub> FET-based inverter, they could also successfully demonstrate a NAND gate, as shown in Fig. 9d-f. As a further potential application, they additionally demonstrated a current mirror, which is a basic component in analogue electronic circuits.

### Inkjet-printed vdW superconducting devices

Until recently, demonstrating superconducting devices by using inkjet printing has been very challenging. Continued efforts have recently encouraged a shift of 2D vdW printing research interest from conventional electronics to unprecedented applications by

fully exploiting the unique properties of 2D vdW materials. In addition, as diverse novel 2D vdW materials have been synthesized and formulated into printable inks with the help of state-of-the-art electrochemical exfoliation methods, Li *et al.* could produce large-area high-quality printable 2D NbSe<sub>2</sub> monolayers and demonstrate superconducting devices by using inkjet printing. By introducing quaternary ammonium cations as a cathodic intercalant, they could successfully exfoliate and formulate Nb(Se/Te)<sub>2</sub>, Ta(S/Se)<sub>2</sub>, Ti(S/Se)<sub>2</sub>, and MoTe<sub>2</sub> inks, as shown on the left side of Fig. 5a.<sup>44</sup> Most importantly, the large size of the 2D flakes facilitates a channel with fewer barriers between the layered flakes when they form a connected conducting channel. In contrast, for electrochemical exfoliation under mild external energy conditions, the general LPE process includes high-power ultrasonication to exfoliate flakes and prevent reaggregation. Consequently, the high-power ultrasonication process will inevitably create additional defects, simultaneously producing small size flakes. In this context, optimized conditions are necessary to exfoliate less defective, larger 2D flakes. Although lithium ions have been widely used for electrochemical LPE methods, intercalated lithium ions have been known to distort lattice structures, changing the crystal phase. However, Li *et al.* could produce high-quality large flakes by alternatively employing tetrabutylammonium cations. The yield of 1-5 layers of the 2D superconducting film was confirmed to be greater than 80%. The lateral dimension of

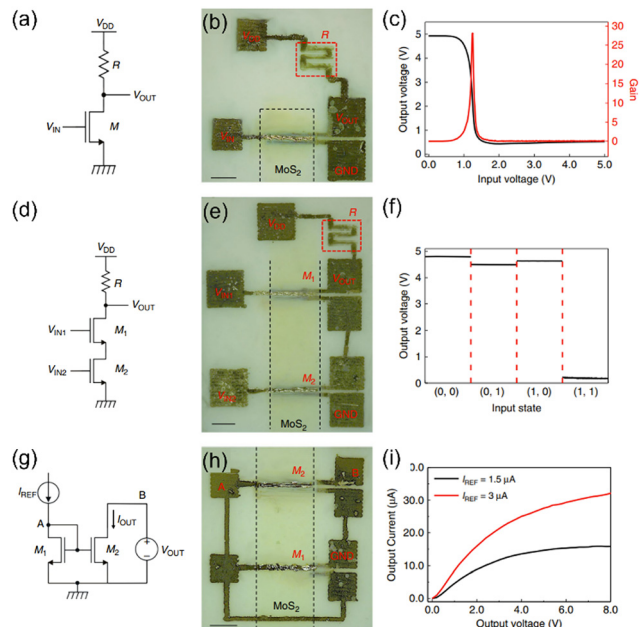


**Fig. 9** (a) Electrical schematic and (b) optical image of an inverter. (c) Output voltage and voltage gain as a function of the input voltage. (d) Electrical schematic and (e) optical image of a NAND gate. (f) Output voltage of the NAND gate as a function of the input states. (g) Electrical schematic and (h) optical image of a current mirror. (i) Output current of the current mirror as a function of the output voltage for two different references. Reproduced under the terms of the Creative Commons CC BY license.<sup>107</sup>

exfoliated NbSe<sub>2</sub> monolayers was found to be larger than a few hundred micrometres (Fig. 10a). Additionally, the quality of the exfoliated flakes was good enough to demonstrate superconducting device applications, as shown in the scanning tunnelling microscopy (STM) image of Fig. 10b. In addition to STM analysis, they also measured the electrical properties of a Hall bar device with an as-exfoliated flake to evaluate the quality of exfoliated flakes. Impurity scattering and defects lead to a large residual resistance (*i.e.*, a small residual resistance ratio (RRR)). The RRR value of electrochemically exfoliated NbSe<sub>2</sub> flakes was determined to be approximately 3.5, which is smaller than that of mechanically exfoliated NbSe<sub>2</sub> but larger than that of CVD-grown flakes, implying less disorder in the electrochemically exfoliated NbSe<sub>2</sub> flakes. Additionally, the superconducting transition temperature of printed NbSe<sub>2</sub> was found to be  $\sim 3.2$  K, as shown in Fig. 10c, which is consistent with the previously reported value. With high-quality 2D vdW inks, the authors could even demonstrate well-operated Josephson junction behaviour. In particular, this novel LPE method not only provides high-quality flakes but also allows the formulation of stable NbSe<sub>2</sub> inks for 2D and even 3D printing processes. In addition, the solvent protection and self-cleaning nature of 2D vdW materials prevent potential degradation of device performance without additional encapsulation layers during the time-consuming fabrication process. As a result, the 3D printed structure, shown in Fig. 10e, showed a diamagnetic transition at  $\sim 6.8$  K, which is a representative signature

of the superconducting transition. The wafer-scale printed NbSe<sub>2</sub> pattern also successfully showed superconducting behaviour, as shown in Fig. 10i–l. Interestingly, the printed NbSe<sub>2</sub> wire showed both bulk-like superconducting transition behaviour and a monolayer-like upper critical field. The authors assumed that this might be due to the mixed effects from Pauli paramagnetism and spin–orbit scattering in NbSe<sub>2</sub> at the interlayer Josephson junctions.

## Challenges and outlook

Despite rapid progress and developments, there are remaining hurdles that should be addressed to fully utilize the inkjet printing strategy for future applications based on 2D vdW materials. First, the printing of a uniform 2D vdW monolayer should be guaranteed because the atomically thin nature of 2D vdW materials is one of the most attractive features. In addition, the absence of dangling bonds on their surfaces reduces the thickness of vdW films down to the atomic scale, which is challenging for conventional 3D semiconductors with a large number of reactive dangling bonds. To successfully employ the advantages of 2D vdW materials, the printed channel should be thinned down to the monolayer limit, although layer-by-layer controlling of the LPE is a remaining issue. Furthermore, a variety of 2D semiconducting vdW materials have a direct bandgap in the monolayer system. Thus, the printing of monolayer 2D vdW materials is also encouraged for optoelectronic applications. From this perspective, many researchers have tried to print a monolayer of 2D materials. As illustrated in Fig. 11a, meeting this demand by adjusting the printing conditions, such as the temperature of the substrate, to control the Marangoni convection and the capillary flow, thus removing excessive liquid, has been attempted.<sup>108</sup> However, the liquid removal process is difficult to employ in the inkjet printing process, and the deposited film was found to have uncovered regions that hinder charge transport. Recently, spin-coating of electrochemically exfoliated vdW materials to obtain vdW layered films was found to be more suitable for depositing uniform 2D vdW films for flexible and stretchable applications than CVD growth of films because shear movement in the lateral direction is allowed due to the weak vdW interaction and network-like morphology, while the CVD-grown film cannot be freely stretched due to the strong in-plane covalent bonding between atoms.<sup>109</sup> This result indicates that a partially staggered structure of monolayer flakes can also be demonstrated by using inkjet printing to deliver stretchability while maintaining the unique properties of monolayer vdW materials. Although the bottom-up synthesis methods are known to produce lower quality 2D materials for the large-area applications so far, these methods can be alternatively used for the monolayer deposition if the remaining quality issue could be addressed, since they have attractive potentials, such as high controllability of surface morphology, crystallite size, and dopant.<sup>110</sup> In addition, the combination of inkjet printing and CVD synthesis can also be a feasible solution to deposit 2D vdW monolayers. Wan *et al.* directly printed the precursor onto the target substrate on demand, which was

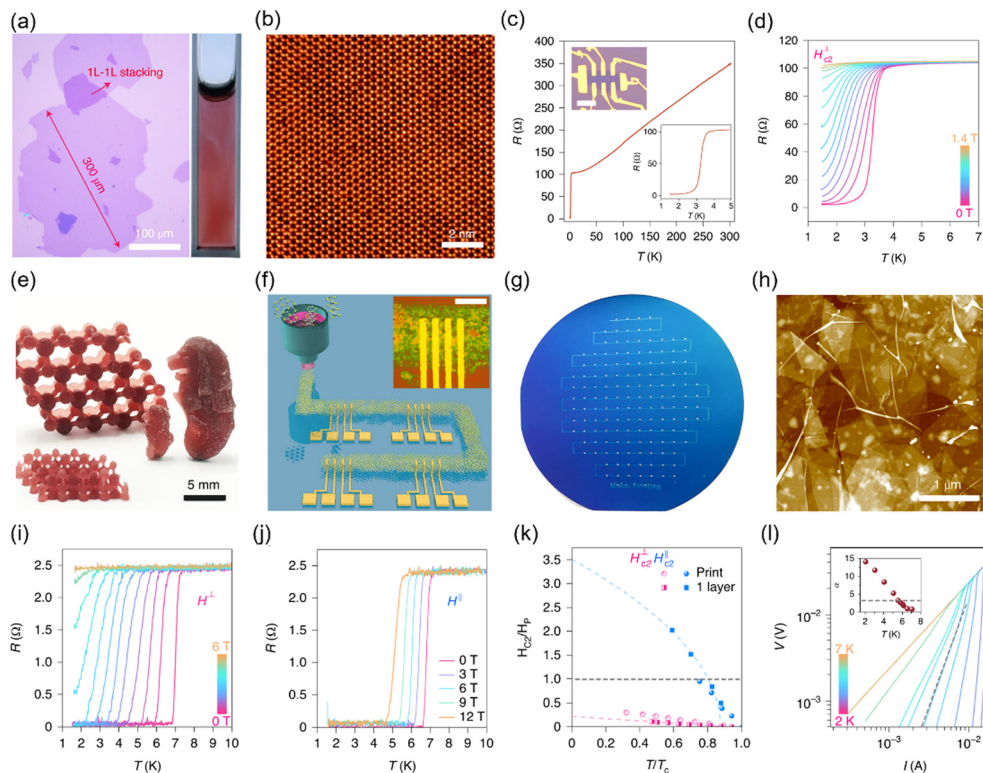


**Fig. 10** (a) Optical image of NbSe<sub>2</sub> monolayer flakes. The right inset shows a photograph of tetrapropylammonium (TPA)-exfoliated NbSe<sub>2</sub> flakes in propylene carbonate (PC). (b) Atomically resolved scanning transmission electron microscopy annular dark-field (STEM-ADF) image of an exfoliated NbSe<sub>2</sub> flake. (c) Temperature-dependent longitudinal resistance for a monolayer NbSe<sub>2</sub> device. (d) Temperature-dependent longitudinal resistance under various perpendicular magnetic fields. (e) Photograph of models fabricated by 3D printing. (f) Schematic illustration, (g) photograph and (h) atomic force microscopy (AFM) image of an inkjet-printed NbSe<sub>2</sub> wire on a 4-inch SiO<sub>2</sub>/Si wafer. (i and j) Temperature-dependent longitudinal resistance of a printed NbSe<sub>2</sub> film under (i) out-of-plane and (j) in-plane magnetic fields. (k) Critical field as a function of transition temperature for printed NbSe<sub>2</sub> under out-of-plane and in-plane magnetic fields. (l) Voltage–current characteristics at different temperatures. Reproduced with permission.<sup>44</sup> Copyright 2021, Publisher Springer Nature.

followed by CVD synthesis to generate a large-area inkjet-printed patterned monolayer MoS<sub>2</sub> film.<sup>111</sup> Although this approach can provide a directly patterned monolayer of MoS<sub>2</sub>, it can only be conducted on limited substrates compatible with a high-temperature process (>750 °C) for CVD synthesis. In addition, multiple passes of printing and an interspersed CVD process would be essential to realize heterostructures, so the sequentially printed precursors and the subsequent CVD process can affect the underlying layers. Thus, a reliable monolayer printing method should be proposed to fully exploit the advantages of 2D vdW materials.

Second, the realization of 2D vdW heterostructures should be obtainable. The ultimate goal of vdW inkjet printing is to continuously manufacture 2D vdW material-based devices with a high degree of design freedom on target substrates. Beyond depositing only single 2D vdW layers, large-area electronic devices, *e.g.*, transistors, memory devices, sensors, and even logics, should be integrated on a substrate in monolithic manufacturing. Therefore, the printing of stacked heterostructures with various types of 2D vdW inks needs to be pursued, considering their rheological and interfacial properties. It should be noted that the interfacial properties between the printed vdW flakes should be also carefully optimized where they can hugely

affect device performance due to their 2D nature. Particularly, the interfaces formed between inter-flakes by inkjet printing can be different from the pristine counterpart existing in the bulk crystals owing to their weak vdW bonding nature along the *z*-axis. In this sense, it is natural to assume that the interfacial properties between inkjet-printed vdW materials could be inferior compared to those of bulk crystals.

Third, environmentally stable printable vdW materials should be investigated. Until now, emerging novel vdW materials have been synthesized, however, their relatively poor air stability can be a critical bottleneck exhibiting rapid degradation of their unique characteristics under ambient conditions. For example, we strongly believe that the applications based on magnetic vdW materials would be realized by using the inkjet printing technique as well in the near future since there have been many efforts to explore vdW magnetic materials, including CrI<sub>3</sub> and Fe<sub>3</sub>GeTe<sub>2</sub>, which have received attention as emerging magnetic vdW materials. Because it would be extremely challenging where such magnetic and topological materials are typically unstable under ambient conditions, so they must only be used in a controlled environment.<sup>112,113</sup> Due to these difficulties, there are barely any demonstrations to date on inkjet printing of 2D vdW materials for magnetism, twistrionics, and other related

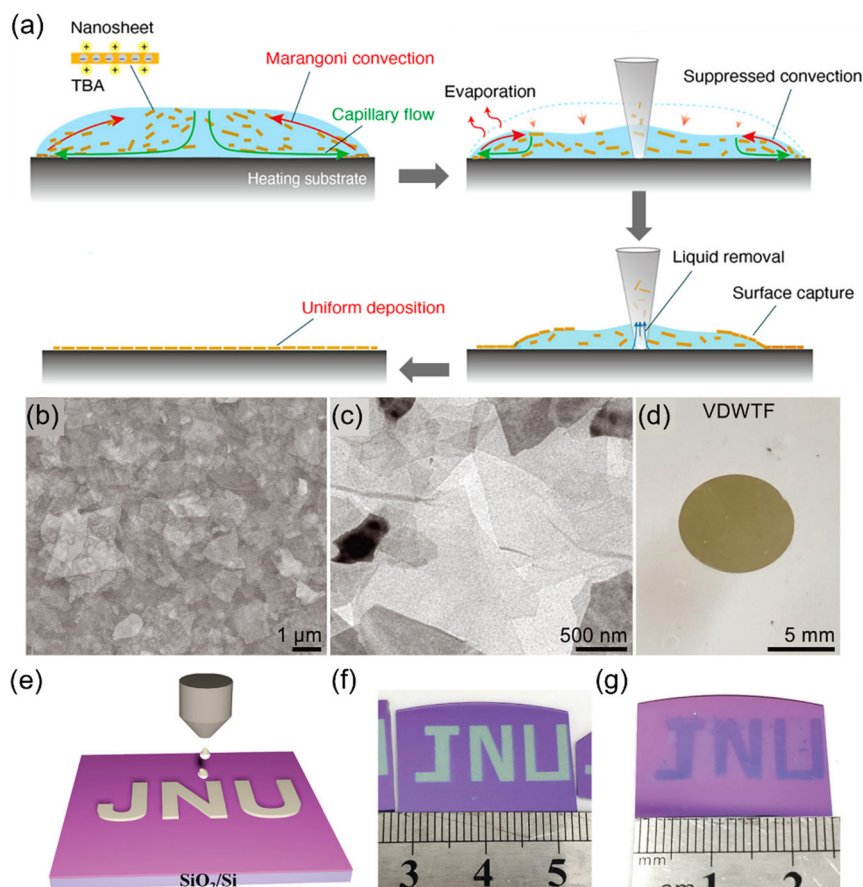


**Fig. 11** (a) Plausible model for 2D nanosheet tiling. Reproduced with permission.<sup>108</sup> Copyright 2020, Publisher ACS. (b) Scanning electron microscopy (SEM) and (c) transmission electron microscopy (TEM) images showing a vdW thin film assembled from staggered 2D nanosheets. (d) Photograph of the vdW thin film floating on water. Reproduced with permission.<sup>109</sup> Copyright 2022, Publisher AAAS. (e) Schematic of printed precursors on a substrate. (f) Photograph of the printed precursor. (g) Photograph of the patterned MoS<sub>2</sub> film after CVD growth. Reproduced with permission.<sup>111</sup> Copyright 2021, Publisher Wiley-VCH.

topics. In addition, the electrical or optoelectronic properties of vdW materials can also be degraded by exposure to solvents. During the continuous inkjet printing process to fabricate vertically stacked heterostructures, the vdW materials will inevitably be exposed to the sequentially dropped ink solvents. Furthermore, as the thickness of vdW materials decreases, *i.e.*, the surface-to-volume ratio increases, the printed vdW materials will be largely affected by the surrounding environment. Thus, introducing suitable additives or binders may be beneficial for stabilizing the printable environment-sensitive vdW materials. Additionally, orthogonal solvents that cannot affect the underlying layers should be used to disperse 2D vdW materials while considering the printability.

In conclusion, 2D vdW materials have shown promising opportunities to demonstrate a new class of electronics compared to other low-dimensional materials. Recently, as practical 2D vdW device applications have been pursued, many research groups have been dedicating much effort, such as employing advanced manufacturing to demonstrate large-area, reliable, and high-performance 2D vdW heterostructures. Owing to the solution processability of 2D vdW materials, inkjet printing has

been rising as a suitable approach for realizing emerging 2D vdW applications. Inkjet printing can pave a promising pathway to produce low-cost and scalable heterostructures with the DOD processability. Although there are remaining challenges, we believe that the attractive advantages of inkjet printing will ensure great synergetic effects with 2D vdW materials, exploiting their unique characteristics, and further improving the quality of life to a higher level.

## Conflicts of interest

There are no conflicts to declare.

## Acknowledgements

The authors appreciate the financial support from the National Research Foundation of Korea (NRF) grant funded by the Korean government (the Ministry of Science and ICT) (No. NRF-2020R1A2C4001948, NRF-2021R1C1C2091728 and NRF-2021R1A2C3004783), and the Korea Institute of Science

and Technology (KIST) Future Resource Research Program (2E31811).

## Notes and references

- S. Han, M. K. Kim, B. Wang, D. S. Wie, S. Wang and C. H. Lee, *Adv. Mater.*, 2016, **28**, 10257–10265.
- D.-M. Drotlef, M. Amjadi, M. Yunusa and M. Sitti, *Adv. Mater.*, 2017, **29**, 1701353.
- A. Koh, D. Kang, Y. Xue, S. Lee, R. M. Pielak, J. Kim, T. Hwang, S. Min, A. Banks, P. Bastien, M. C. Manco, L. Wang, K. R. Ammann, K.-I. Jang, P. Won, S. Han, R. Ghaffari, U. Paik, M. J. Slepian, G. Balooch, Y. Huang and J. A. Rogers, *Sci. Transl. Med.*, 2016, **8**, 366ra165.
- S. Imani, A. J. Bandodkar, A. M. V. Mohan, R. Kumar, S. Yu, J. Wang and P. P. Mercier, *Nat. Commun.*, 2016, **7**, 11650.
- W. Gao, S. Emaminejad, H. Y. Y. Nyein, S. Challa, K. Chen, A. Peck, H. M. Fahad, H. Ota, H. Shiraki, D. Kiriya, D.-H. Lien, G. A. Brooks, R. W. Davis and A. Javey, *Nature*, 2016, **529**, 509–514.
- L. Pi, L. Li, K. Liu, Q. Zhang, H. Li and T. Zhai, *Adv. Funct. Mater.*, 2019, **29**, 1904932.
- M. Och, M.-B. Martin, B. Dlubak, P. Seneor and C. Mattevi, *Nanoscale*, 2021, **13**, 2157–2180.
- K. Cho, J. Pak, S. Chung and T. Lee, *ACS Nano*, 2019, **13**, 9713–9734.
- K. S. Burch, D. Mandrus and J.-K. Park, *Nature*, 2018, **563**, 47–52.
- A. H. Castro Neto, F. Guinea, N. M. R. Peres, K. S. Novoselov and A. K. Geim, *Rev. Mod. Phys.*, 2009, **81**, 109–162.
- K. S. Novoselov, A. Mishchenko, A. Carvalho and A. H. Castro Neto, *Science*, 2016, **353**, aac9439.
- M. Gibertini, M. Koperski, A. F. Morpurgo and K. S. Novoselov, *Nat. Nanotechnol.*, 2019, **14**, 408–419.
- D. Jariwala, V. K. Sangwan, L. J. Lauhon, T. J. Marks and M. C. Hersam, *ACS Nano*, 2014, **8**, 1102–1120.
- G. Fiori, F. Bonaccorso, G. Iannaccone, T. Palacios, D. Neumaier, A. Seabaugh, S. K. Banerjee and L. Colombo, *Nat. Nanotechnol.*, 2014, **9**, 768–779.
- S. J. Kim, K. Choi, B. Lee, Y. Kim and B. H. Hong, *Annu. Rev. Mater. Res.*, 2015, **45**, 63–84.
- Q. H. Wang, K. Kalantar-Zadeh, A. Kis, J. N. Coleman and M. S. Strano, *Nat. Nanotechnol.*, 2012, **7**, 699–712.
- C.-C. Chiang, V. Ostwal, P. Wu, C.-S. Pang, F. Zhang, Z. Chen and J. Appenzeller, *Appl. Phys. Rev.*, 2021, **8**, 021306.
- J. Li, M. C. Lemme and M. Östling, *Chem. Phys. Chem.*, 2014, **15**, 3427–3434.
- R. Worsley, L. Pimpolari, D. McManus, N. Ge, R. Ionescu, J. A. Wittkopf, A. Alieva, G. Basso, M. Macucci, G. Iannaccone, K. S. Novoselov, H. Holder, G. Fiori and C. Casiraghi, *ACS Nano*, 2019, **13**, 54–60.
- K. Hassan, M. J. Nine, T. T. Tung, N. Stanley, P. L. Yap, H. Rastin, L. Yu and D. Losic, *Nanoscale*, 2020, **12**, 19007–19042.
- G. Hu, J. Kang, L. W. T. Ng, X. Zhu, R. C. T. Howe, C. G. Jones, M. C. Hersam and T. Hasan, *Chem. Soc. Rev.*, 2018, **47**, 3265–3300.
- A. Capasso, A. E. Del Rio Castillo, H. Sun, A. Ansaldo, V. Pellegrini and F. Bonaccorso, *Solid State Commun.*, 2015, **224**, 53–63.
- L. W. T. Ng, G. Hu, R. C. T. Howe, X. Zhu, Z. Yang, C. G. Jones and T. Hasan, *Printing of Graphene and Related 2D Materials: Technology, Formulation and Applications*, Springer International Publishing, Cham, 2019.
- J. Liang, C. Jiang and W. Wu, *Appl. Phys. Rev.*, 2021, **8**, 021319.
- R. Yang, J. Zhou, C. Yang, L. Qiu and H. Cheng, *Adv. Mater. Technol.*, 2020, **5**, 1901066.
- S. Chung, K. Cho and T. Lee, *Adv. Sci.*, 2019, **6**, 1801445.
- Z. Lin, Y. Huang and X. Duan, *Nat. Electron.*, 2019, **2**, 378–388.
- E. Cannavò, D. Marian, E. G. Marín, G. Iannaccone and G. Fiori, *Phys. Rev. B*, 2021, **104**, 085433.
- F. Wang, J. H. Gosling, G. F. Trindade, G. A. Rance, O. Makarovskiy, N. D. Cottam, Z. Kudrynskiy, A. G. Balanov, M. T. Greenaway, R. D. Wildman, R. Hague, C. Tuck, T. M. Fromhold and L. Turyanska, *Adv. Funct. Mater.*, 2021, **31**, 2007478.
- S. Lu and A. D. Franklin, *Nanoscale*, 2020, **12**, 23371–23390.
- J. Zhou, J. Lin, X. Huang, Y. Zhou, Y. Chen, J. Xia, H. Wang, Y. Xie, H. Yu, J. Lei, D. Wu, F. Liu, Q. Fu, Q. Zeng, C.-H. Hsu, C. Yang, L. Lu, T. Yu, Z. Shen, H. Lin, B. I. Yakobson, Q. Liu, K. Suenaga, G. Liu and Z. Liu, *Nature*, 2018, **556**, 355–359.
- J.-W. T. Seo, J. Zhu, V. K. Sangwan, E. B. Secor, S. G. Wallace and M. C. Hersam, *ACS Appl. Mater. Interfaces*, 2019, **11**, 5675–5681.
- T. Carey, S. Cacovich, G. Divitini, J. Ren, A. Mansouri, J. M. Kim, C. Wang, C. Ducati, R. Sordan and F. Torrisi, *Nat. Commun.*, 2017, **8**, 1202.
- R. F. Hossain, M. Min and A. B. Kaul, *MRS Adv.*, 2019, **4**, 621–627.
- D. J. Finn, M. Lotya, G. Cunningham, R. J. Smith, D. McCloskey, J. F. Donegan and J. N. Coleman, *J. Mater. Chem. C*, 2014, **2**, 925–932.
- C. Casiraghi, M. Macucci, K. Parvez, R. Worsley, Y. Shin, F. Bronte, C. Borri, M. Paggi and G. Fiori, *Carbon*, 2018, **129**, 462–467.
- T. Juntunen, H. Jussila, M. Ruoho, S. Liu, G. Hu, T. Albrow-Owen, L. W. T. Ng, R. C. T. Howe, T. Hasan, Z. Sun and I. Tittonen, *Adv. Funct. Mater.*, 2018, **28**, 1800480.
- J. Li, F. Rossignol and J. Macdonald, *Lab Chip*, 2015, **15**, 2538–2558.
- E. B. Secor, P. L. Prabhmirashi, K. Puntambekar, M. L. Geier and M. C. Hersam, *J. Phys. Chem. Lett.*, 2013, **4**, 1347–1351.
- J. Li, M. M. Naiini, S. Vaziri, M. C. Lemme and M. Östling, *Adv. Funct. Mater.*, 2014, **24**, 6524–6531.
- P. He and B. Derby, *2D Mater.*, 2017, **4**, 021021.
- F. Torrisi, T. Hasan, W. Wu, Z. Sun, A. Lombardo, T. S. Kulmala, G.-W. Hsieh, S. Jung, F. Bonaccorso, P. J. Paul, D. Chu and A. C. Ferrari, *ACS Nano*, 2012, **6**, 2992–3006.

- 43 X. Jiang, W. Li, T. Hai, R. Yue, Z. Chen, C. Lao, Y. Ge, G. Xie, Q. Wen and H. Zhang, *npj 2D Mater. Appl.*, 2019, **3**, 34.
- 44 J. Li, P. Song, J. Zhao, K. Vaklinova, X. Zhao, Z. Li, Z. Qiu, Z. Wang, L. Lin, M. Zhao, T. S. Herng, Y. Zuo, W. Jonhson, W. Yu, X. Hai, P. Lyu, H. Xu, H. Yang, C. Chen, S. J. Pennycook, J. Ding, J. Teng, A. H. Castro Neto, K. S. Novoselov and J. Lu, *Nat. Mater.*, 2021, **20**, 181–187.
- 45 A. G. Kelly, T. Hallam, C. Backes, A. Harvey, A. S. Esmaily, I. Godwin, J. Coelho, V. Nicolosi, J. Lauth, A. Kulkarni, S. Kinge, L. D. A. Siebbeles, G. S. Duesberg and J. N. Coleman, *Science*, 2017, **356**, 69–73.
- 46 T.-Y. Kim, J. Ha, K. Cho, J. Pak, J. Seo, J. Park, J.-K. Kim, S. Chung, Y. Hong and T. Lee, *ACS Nano*, 2017, **11**, 10273–10280.
- 47 Y. Zhang, T.-R. Chang, B. Zhou, Y.-T. Cui, H. Yan, Z. Liu, F. Schmitt, J. Lee, R. Moore, Y. Chen, H. Lin, H.-T. Jeng, S.-K. Mo, Z. Hussain, A. Bansil and Z.-X. Shen, *Nat. Nanotechnol.*, 2014, **9**, 111–115.
- 48 J. Su, M. Wang, G. Liu, H. Li, J. Han and T. Zhai, *Adv. Sci.*, 2020, **7**, 2001722.
- 49 D. Dumcenco and E. Giannini, *J. Cryst. Growth*, 2020, **548**, 125799.
- 50 M. Tanaka, Y. Fujishiro, M. Mogi, Y. Kaneko, T. Yokosawa, N. Kanazawa, S. Minami, T. Koretsune, R. Arita, S. Tarucha, M. Yamamoto and Y. Tokura, *Nano Lett.*, 2020, **20**, 7476–7481.
- 51 D. Hu, G. Xu, L. Xing, X. Yan, J. Wang, J. Zheng, Z. Lu, P. Wang, X. Pan and L. Jiao, *Angew. Chem.*, 2017, **129**, 3665–3669.
- 52 L. Wang, I. Meric, P. Y. Huang, Q. Gao, Y. Gao, H. Tran, T. Taniguchi, K. Watanabe, L. M. Campos, D. A. Muller, J. Guo, P. Kim, J. Hone, K. L. Shepard and C. R. Dean, *Science*, 2013, **342**, 614–617.
- 53 X. Cui, G.-H. Lee, Y. D. Kim, G. Arefe, P. Y. Huang, C.-H. Lee, D. A. Chenet, X. Zhang, L. Wang, F. Ye, F. Pizzocchero, B. S. Jessen, K. Watanabe, T. Taniguchi, D. A. Muller, T. Low, P. Kim and J. Hone, *Nat. Nanotechnol.*, 2015, **10**, 534–540.
- 54 B. Radisavljevic, A. Radenovic, J. Brivio, V. Giacometti and A. Kis, *Nat. Nanotechnol.*, 2011, **6**, 147–150.
- 55 J.-K. Kim, K. Cho, J. Jang, K.-Y. Baek, J. Kim, J. Seo, M. Song, J. Shin, J. Kim, S. S. Parkin, J.-H. Lee, K. Kang and T. Lee, *Adv. Mater.*, 2021, **33**, 2101598.
- 56 B. Huang, G. Clark, D. R. Klein, D. MacNeill, E. Navarro-Moratalla, K. L. Seyler, N. Wilson, M. A. McGuire, D. H. Cobden, D. Xiao, W. Yao, P. Jarillo-Herrero and X. Xu, *Nat. Nanotechnol.*, 2018, **13**, 544–548.
- 57 L. Webster and J.-A. Yan, *Phys. Rev. B*, 2018, **98**, 144411.
- 58 Y. Deng, Y. Yu, Y. Song, J. Zhang, N. Z. Wang, Z. Sun, Y. Yi, Y. Z. Wu, S. Wu, J. Zhu, J. Wang, X. H. Chen and Y. Zhang, *Nature*, 2018, **563**, 94–99.
- 59 M. M. Ugeda, A. J. Bradley, Y. Zhang, S. Onishi, Y. Chen, W. Ruan, C. Ojeda-Aristizabal, H. Ryu, M. T. Edmonds, H.-Z. Tsai, A. Riss, S.-K. Mo, D. Lee, A. Zettl, Z. Hussain, Z.-X. Shen and M. F. Crommie, *Nat. Phys.*, 2016, **12**, 92–97.
- 60 X. Xi, L. Zhao, Z. Wang, H. Berger, L. Forró, J. Shan and K. F. Mak, *Nat. Nanotechnol.*, 2015, **10**, 765–769.
- 61 K.-R. Jeon, K. Cho, A. Chakraborty, J.-C. Jeon, J. Yoon, H. Han, J.-K. Kim and S. S. Parkin, *ACS Nano*, 2021, **15**, 16819–16827.
- 62 P. Zareapour, A. Hayat, S. Y. F. Zhao, M. Kreshchuk, A. Jain, D. C. Kwok, N. Lee, S.-W. Cheong, Z. Xu, A. Yang, G. D. Gu, S. Jia, R. J. Cava and K. S. Burch, *Nat. Commun.*, 2012, **3**, 1056.
- 63 W. Liao, S. Zhao, F. Li, C. Wang, Y. Ge, H. Wang, S. Wang and H. Zhang, *Nanoscale Horiz.*, 2020, **5**, 787–807.
- 64 Y. Liu, N. O. Weiss, X. Duan, H.-C. Cheng, Y. Huang and X. Duan, *Nat. Rev. Mater.*, 2016, **1**, 1–17.
- 65 A. Chaves, J. G. Azadani, H. Alsalman, D. R. da Costa, R. Frisenda, A. J. Chaves, S. H. Song, Y. D. Kim, D. He, J. Zhou, A. Castellanos-Gomez, F. M. Peeters, Z. Liu, C. L. Hinkle, S.-H. Oh, P. D. Ye, S. J. Koester, Y. H. Lee, P. Avouris, X. Wang and T. Low, *npj 2D Mater. Appl.*, 2020, **4**, 29.
- 66 K. Yasuda, X. Wang, K. Watanabe, T. Taniguchi and P. Jarillo-Herrero, *Science*, 2021, **372**, 1458–1462.
- 67 A. Weston, E. G. Castanon, V. Enaldiev, F. Ferreira, S. Bhattacharjee, S. Xu, H. Corte-León, Z. Wu, N. Clark, A. Summerfield, T. Hashimoto, Y. Gao, W. Wang, M. Hamer, H. Read, L. Fumagalli, A. V. Kretinin, S. J. Haigh, O. Kazakova, A. K. Geim, V. I. Fal'ko and R. Gorbachev, *Nat. Nanotechnol.*, 2022, 1–6.
- 68 Y. Cao, V. Fatemi, S. Fang, K. Watanabe, T. Taniguchi, E. Kaxiras and P. Jarillo-Herrero, *Nature*, 2018, **556**, 43–50.
- 69 R. Frisenda, E. Navarro-Moratalla, P. Gant, D. P. D. Lara, P. Jarillo-Herrero, R. V. Gorbachev and A. Castellanos-Gomez, *Chem. Soc. Rev.*, 2018, **47**, 53–68.
- 70 J. F. Sierra, J. Fabian, R. K. Kawakami, S. Roche and S. O. Valenzuela, *Nat. Nanotechnol.*, 2021, **16**, 856–868.
- 71 W. Han, *APL Mater.*, 2016, **4**, 032401.
- 72 X. Lin, W. Yang, K. L. Wang and W. Zhao, *Nat. Electron.*, 2019, **2**, 274–283.
- 73 Y. Zhou and L.-D. Zhao, *Adv. Mater.*, 2017, **29**, 1702676.
- 74 K. Kanahashi, J. Pu and T. Takenobu, *Adv. Energy Mater.*, 2020, **10**, 1902842.
- 75 C. Bao, P. Tang, D. Sun and S. Zhou, *Nat. Rev. Phys.*, 2022, **4**, 33–48.
- 76 Y. Deng, Y. Yu, M. Z. Shi, Z. Guo, Z. Xu, J. Wang, X. H. Chen and Y. Zhang, *Science*, 2020, **367**, 895–900.
- 77 A. A. Soluyanov, D. Gresch, Z. Wang, Q. Wu, M. Troyer, X. Dai and B. A. Bernevig, *Nature*, 2015, **527**, 495–498.
- 78 M. Blei, J. L. Lado, Q. Song, D. Dey, O. Erten, V. Pardo, R. Comin, S. Tongay and A. S. Botana, *Appl. Phys. Rev.*, 2021, **8**, 021301.
- 79 L. Zhang, J. Zhou, H. Li, L. Shen and Y. P. Feng, *Appl. Phys. Rev.*, 2021, **8**, 021308.
- 80 J. Yao and G. Yang, *Adv. Sci.*, 2022, **9**, 2103036.
- 81 A. Ciesielskia and P. Samori, *Chem. Soc. Rev.*, 2014, **43**, 381–398.
- 82 Y. Hernandez, V. Nicolosi, M. Lotya, F. M. Blighe, Z. Sun, S. De, I. T. McGovern, B. Holland, M. Byrne, Y. K. Gun'Ko,

- J. J. Boland, P. Niraj, G. Duesberg, S. Krishnamurthy, R. Goodhue, J. Hutchison, V. Scardaci, A. C. Ferrari and J. N. Coleman, *Nat. Nanotechnol.*, 2008, **3**, 563–568.
- 83 Y. Yang, X. Ji, X. Yang, C. Wang, W. Song, Q. Chen and C. E. Banks, *RSC Adv.*, 2013, **3**, 16130.
- 84 L. Li, D. Zhang, Y. Gao, J. Deng, Y. Gou and J. Fang, *J. Alloys Compd.*, 2021, **862**, 158551.
- 85 A. Ambrosi and M. Pumera, *Chem. Soc. Rev.*, 2018, **47**, 7213–7224.
- 86 S. Yang, S. Brüller, Z.-S. Wu, Z. Liu, K. Parvez, R. Dong, F. Richard, P. Samorì, X. Feng and K. Müllen, *J. Am. Chem. Soc.*, 2015, **137**, 13927–13932.
- 87 T. C. Achee, W. Sun, J. T. Hope, S. G. Quitzau, C. B. Sweeney, S. A. Shah, T. Habib and M. J. Green, *Sci. Rep.*, 2018, **8**, 14525.
- 88 H. Lee, M. Koo, C. Park, M. Patel, H. Han, T. H. Park, P. Kumar, W.-G. Koh and C. Park, *Nano Res.*, 2020, **13**, 2726–2734.
- 89 L. Li, D. Zhang, Y. Gao, J. Deng, Y. Gou and J. Fang, *J. Alloys Compd.*, 2021, **862**, 158551.
- 90 B.-J. de Gans, P. C. Duineveld and U. S. Schubert, *Adv. Mater.*, 2004, **16**, 203–213.
- 91 N. C. Raut and K. Al-Shamery, *J. Mater. Chem. C*, 2018, **6**, 1618–1641.
- 92 B. Derby, *Annu. Rev. Mater. Res.*, 2010, **40**, 395–414.
- 93 K. Kouroupis-Agalou, A. Liscio, E. Treossi, L. Ortolani, V. Morandi, N. Maria Pugno and V. Palermo, *Nanoscale*, 2014, **6**, 5926–5933.
- 94 X. Liu, T.-J. Tarn, F. Huang and J. Fan, *Particuology*, 2015, **19**, 1–13.
- 95 J. E. Fromm, *IBM J. Res. Dev.*, 1984, **28**, 322–333.
- 96 S. Mueller, E. W. Llewellyn and H. M. Mader, *Proc. R. Soc. A*, 2010, **466**, 1201–1228.
- 97 N. Reis and B. Derby, *Mater. Res. Soc. Symp. Proc.*, 2000, **624**, 65–70.
- 98 D. McManus, S. Vranic, F. Withers, V. Sanchez-Romaguera, M. Macucci, H. Yang, R. Sorrentino, K. Parvez, S.-K. Son, G. Iannaccone, K. Kostarelos, G. Fiori and C. Casiraghi, *Nat. Nanotechnol.*, 2017, **12**, 343–350.
- 99 M. Zeng, W. Kuang, I. Khan, D. Huang, Y. Du, M. Saeidi-Javash, L. Zhang, Z. Cheng, A. J. Hoffman and Y. Zhang, *Adv. Mater.*, 2020, **32**, 2003081.
- 100 T.-Y. Kim, M. Amani, G. H. Ahn, Y. Song, A. Javey, S. Chung and T. Lee, *ACS Nano*, 2016, **10**, 2819–2826.
- 101 W. Zheng, F. Saiz, Y. Shen, K. Zhu, Y. Liu, C. McAleese, B. Conran, X. Wang and M. Lanza, *Adv. Mater.*, 2021, 2104138.
- 102 S. Bang, S. Lee, A. Rai, N. T. Duong, I. Kawk, S. Wolf, C.-H. Chung, S. K. Banerjee, A. C. Kummel, M. S. Jeong and J. H. Park, *Adv. Funct. Mater.*, 2020, **30**, 2000250.
- 103 D. S. Schulman, A. J. Arnold and S. Das, *Chem. Soc. Rev.*, 2018, **47**, 3037–3058.
- 104 A. Allain, J. Kang, K. Banerjee and A. Kis, *Nat. Mater.*, 2015, **14**, 1195–1205.
- 105 K. Cho, J. Pak, J.-K. Kim, K. Kang, T.-Y. Kim, J. Shin, B. Y. Choi, S. Chung and T. Lee, *Adv. Mater.*, 2018, **30**, 1705540.
- 106 Y. Liu, J. Guo, E. Zhu, L. Liao, S.-J. Lee, M. Ding, I. Shakir, V. Gambin, Y. Huang and X. Duan, *Nature*, 2018, **557**, 696–700.
- 107 S. Conti, L. Pimpolari, G. Calabrese, R. Worsley, S. Majee, D. K. Polyushkin, M. Paur, S. Pace, D. H. Keum, F. Fabbri, G. Iannaccone, M. Macucci, C. Coletti, T. Mueller, C. Casiraghi and G. Fiori, *Nat. Commun.*, 2020, **11**, 3566.
- 108 Y. Shi, M. Osada, Y. Ebina and T. Sasaki, *ACS Nano*, 2020, **14**, 15216–15226.
- 109 Z. Yan, D. Xu, Z. Lin, P. Wang, B. Cao, H. Ren, F. Song, C. Wan, L. Wang, J. Zhou, X. Zhao, J. Chen, Y. Huang and X. Duan, *Science*, 2022, **375**, 852–859.
- 110 S. H. Choi, S. J. Yun, Y. S. Won, C. S. Oh, S. M. Kim, K. K. Kim and Y. H. Lee, *Nat. Commun.*, 2022, **13**, 1484.
- 111 X. Wan, X. Miao, J. Yao, S. Wang, F. Shao, S. Xiao, R. Zhan, K. Chen, X. Zeng, X. Gu and J. Xu, *Adv. Mater.*, 2021, **33**, 2100260.
- 112 D. Shcherbakov, P. Stepanov, D. Weber, Y. Wang, J. Hu, Y. Zhu, K. Watanabe, T. Taniguchi, Z. Mao, W. Windl, J. Goldberger, M. Bockrath and C. N. Lau, *Nano Lett.*, 2018, **18**, 4214–4219.
- 113 D. Kim, S. Park, J. Lee, J. Yoon, S. Jook, T. Kim, K. Min, S.-Y. Park, C. Kim, K.-W. Moon, C. Lee, J. Hong and C. Hwang, *Nanotechnology*, 2019, **30**, 245701.